Materials Chemistry and Physics 154 (2015) 107–117

Contents lists available at ScienceDirect

Materials Chemistry and Physics

journal homepage: www.elsevier.com/locate/matchemphys

Interfacial reaction mechanism between matrix and reinforcement in B_4C/6061Al composites

Y.Z. Li [a], Q.Z. Wang [b, *], W.G. Wang [a], B.L. Xiao [a], Z.Y. Ma [a, *]

[a] Shenyang National Laboratory for Materials Science, Institute of Metal Research, Chinese Academy of Sciences, 72 Wenhua Road, Shenyang 110016, China
[b] Key Laboratory of Nuclear Materials and Safety Assessment, Institute of Metal Research, Chinese Academy of Sciences, 72 Wenhua Road, Shenyang 110016, China

HIGHLIGHTS

- Complicated interfacial reactions occurred in B_4C/6061Al composites.
- Reactions involving Mg and Si were divided into oxidation of Mg and other reactions.
- Al/B_4C reaction produced free B and then activated B/Mg reactions.
- B/Mg reactions rather than Mg oxidation were main reasons for Mg consumption.
- Interfacial reactions definitely deteriorate age-hardening ability of composites.

ARTICLE INFO

Article history:
Received 27 September 2014
Received in revised form
12 December 2014
Accepted 25 January 2015
Available online 27 January 2015

Keywords:
Composite materials
Powder metallurgy
Electron microscopy
Microstructure

ABSTRACT

The interfacial reaction mechanism in B_4C/6061Al composites, fabricated by the powder metallurgy technique at 560 and 620 °C with various holding times, was subjected to detailed investigations using optical microscopy, scanning electron microscopy, transmission electron microscopy, X-ray diffraction and hardness tests. Results showed that complicated interfacial reactions occurred in the B_4C/6061Al composites, forming Al_3BC, $MgAl_2O_4$, MgB_7, $Mg_{0.78}Al_{0.75}B_{14}$, $AlB_{12}C_2$ and Al_4SiC_4 as the main products, which clearly deteriorated the age-hardening ability of the composites. The interfacial reactions involving Mg and Si could be divided into two series. The oxidation of Mg occurred at both 560 and 620 °C, whereas other reactions only occurred at 620 °C. The existence of the liquid phase at 620 °C activated the reaction between Al and B_4C, leading to the generation of free B, and subsequent reactions involving B and Mg occurred. After the reactions involving B and Mg was completed, the reaction involving Al, Si and C took place. It was determined that the reactions involving B and Mg rather than the oxidation of Mg or the reaction involving Si were the main reasons for the consumption of Mg and the deterioration of age-hardening ability of the B_4C/6061Al composites at 620 °C.

© 2015 Elsevier B.V. All rights reserved.

1. Introduction

The interfacial reactions are critical factors influencing the mechanical properties of metal matrix composites [1,2]. For aluminum matrix composites (AMCs), the interfacial reactions occurred not only between Al and the reinforcement, but also among alloying elements (such as Mg, Si, Cu) and the reinforcements. These reactions would definitely change the characteristics of the composites.

First, these reactions would influence the interfacial bonding strength, thereby changing the mechanical properties of the composites [3–5]. Second, the reactions among alloying elements and the reinforcements would vary the composition of the matrix [6–9]. For aging hardenable aluminum alloys, these reactions would change the aging behavior of the composites, leading to obvious changes of the mechanical properties [4,9]. As a consequence, optimization of the mechanical properties of AMCs requires a thorough understanding of the interfacial reactions in these materials.

For the Al–B_4C composite system, the investigations of the

* Corresponding authors.
E-mail addresses: qzwang@imr.ac.cn (Q.Z. Wang), zyma@imr.ac.cn (Z.Y. Ma).

http://dx.doi.org/10.1016/j.matchemphys.2015.01.052
0254-0584/© 2015 Elsevier B.V. All rights reserved.

interfacial reactions are limited with most of studies focused on the reaction between liquid aluminum and B_4C [10–13]. However, the results of these studies were in dispute. For example, while some experimental results showed that the reaction between Al and B_4C requires temperatures of 660 °C at the minimum [10], some investigators verified that the reaction could occur at temperatures as low as 600 °C [11,12]. The major interfacial reaction products were determined to be either AlB_2 [10,13], Al_3BC [10,12] or $AlB_{24}C_2$ [14]. However, the interfacial reactions involving alloying elements and their influence on the aging behavior were rarely reported.

Aging is a common heat treatment method to improve the mechanical properties of AMCs. The age-hardening behavior of AMCs has been the subject of a number of investigations. Some researchers reported the formation of MgO or $MgAl_2O_4$ in Mg containing AMCs [14,15], but did not mention its effect on the aging behavior. Hu [16] suggested that reactions involving Mg possibly had a negative impact on the aging hardenability of B_4C/Al composites, but they did not provide experimental evidence and detailed discussion. More importantly, the interfacial reaction mechanism was not revealed in previous investigations.

In our previous study [17], B_4C/6061Al composites were successfully fabricated by powder metallurgy (PM) technique at temperatures between the solidus and liquidus temperatures of the matrix alloy. Significant deterioration in the age-hardening ability of the B_4C/6061Al composites was observed with slight change of the fabrication parameters, which was definitely different from previous studies. This was attributed to the occurrence of the interfacial reactions involving alloying elements in 6061Al alloy. However, the detailed reaction type and mechanism has not been determined in that study.

In this work, the process of liquid phase formation and the interfacial reactions of the B_4C/6061Al composites were investigated during hot pressing (HP) with different temperatures and holding times. The aim of this study is to understand the interfacial reaction mechanism of the B_4C/6061Al composites. This will be beneficial to establishing optimized HP procedure to produce high performance B_4C/Al composites.

2. Experimental

B_4C/6061Al composites were fabricated by PM technique using 6061Al alloy with a nominal composition of Al–1.0Mg–0.65Si–0.25Cu (wt%) as the matrix and B_4C with an addition of 20 wt% as the reinforcement. The mean sizes of Al powder (99.9 pct. purity, Angang Group Aluminum Powder Co., Ltd.) and B_4C particles (96.5 pct. purity, Mudanjiang Jingangzuan Boron Carbide Co., Ltd.) were 13 and 7 μm, respectively. The B_4C particles exhibited a polygonal morphology with blunt edge and low aspect ratio, as shown in Fig. 1. The main impurities were Al_2O_3 in the Al powder, free B, C and some oxides in the B_4C powders as shown in Table 1.

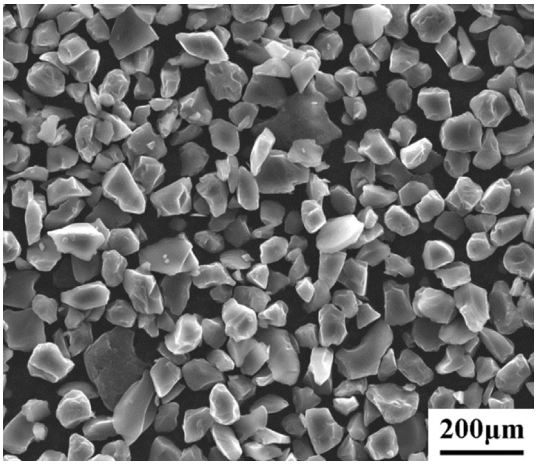

Fig. 1. The morphology of as-received B_4C particles.

The as-received B_4C particles were dried at 150 °C for 8 h, and then mechanically mixed with the Al powder for 8 h in a bi-axis rotary mixer with a rotation speed of 50 rpm. The mixed powders were cold compacted into billets with a height of 60 mm and a diameter of 55 mm in a steel die under a pressure of 20 MPa. Then the compacts were pressed at a pressure of 50 MPa in a vacuum chamber of 10^{-2} Pa with different hot-pressing temperatures and holding times. Part of the billets with the dies was water quenched during the HP process to freeze the microstructure at different stages of HP. The cooling time of the billets with the dies from hot-pressing temperature to room temperature was measured to be about 15 s. Part of the HP billets was forged to discs about 12 mm in thickness at 480 °C. The specifications of the composite samples in this study are shown in Table 2.

The specimens for microstructural examinations were ground with 2000 grit abrasive paper and then mechanically polished. The specimens were observed using optical microscopy (OM, Zeiss Axiovert 200MAT) and scanning electron microscopy (SEM, Quanta 600). The phase analyses were conducted using an X-ray diffraction (XRD) analyzer (D/max 2400). The interface microstructure was examined by transmission electron microscopy (TEM, TECNAI G2 F20). The thin foils for TEM were prepared by ion-milling technique. The compositions of the phases and the matrix of the composites were determined by energy-dispersive spectrometry (EDS). The elemental distribution in the composites was examined by electron probe micro analysis (EPMA-1610) and secondary ion mass spectroscopy (SIMS).

To characterize the interfacial reaction products in more details, B_4C particles with the reaction products were extracted from some of the samples using electrochemical dissolution method. Owing to the hydrophilic nature of some reaction products, the electrolyte used was a solution of HNO_3 (30 vol.%) in methanol. To observe the interfacial reaction products at high magnifications, the extracted particles were coated with 60–80 Å-thick Pt and then examined by field emission scanning electron microscopy (FESEM, Leo Supra 35). The interfacial reaction products in the as-extracted particles were identified by XRD. For the purpose of comparison, the as-received B_4C particles were also examined by XRD. Semi-quantitative analyses were also performed to evaluate the variations of the relative abundances of different phases by measuring the intensities of three characteristic diffraction lines free of overlap and by comparing the values thus obtained from one sample to another [18,19].

To evaluate the effect of the interfacial reactions on the mechanical property, the age hardening behavior of the composites fabricated in different parameters were characterized using Rockwell hardness measurement. These samples were solution treated at 530 °C for 2.5 h, water quenched, and then aged at 175 °C from 0 to 20 h. Six specimens per condition were measured to ensure accuracy of results.

Table 1
The main oxide impurities in Al and B_4C powders.

Al	B_4C	
Al_2O_3 0.1 wt%	B_2O_3 0.4 wt%	Fe_2O_3 0.42 wt%

Table 2
The specifications of the samples in this study.

Code	HP temperature	Holding time at HP temperature	Cooling method after HP
560-2-FC	560 °C	2 h	Furnace cooling
560-10-FC	560 °C	10 h	Furnace cooling
620-2-FC	620 °C	2 h	Furnace cooling
620-0-WQ	620 °C	0 h	Water quenching
620-0.5-WQ	620 °C	0.5 h	Water quenching
620-1-WQ	620 °C	1 h	Water quenching
620-2-WQ	620 °C	2 h	Water quenching

3. Results

3.1. Microstructural characterization of B_4C/6061Al composites

20 wt%B_4C/6061Al composites were fabricated successfully with the same process route but different parameters. Fig. 2 shows the OM micrographs of samples 560-2-FC and 620-2-FC. It can be seen that the hot-pressed temperature did not affect the distribution of the B_4C particles, though the liquid phase fraction during the HP process was different. No porosity was detected in both the composites.

Fig. 3 shows the SEM micrograph of samples 560-2-FC and 620-2-FC. Still no porosity was detected in the composites even under such a high-magnification. While no obvious changes of the B_4C particle morphologies were observed under SEM for these two composites, significant microstructure difference was revealed in the matrix. For sample 560-2-FC with an HP temperature of 560 °C, a relatively clean matrix was observed, as shown in Fig. 3(a). However, when the fabrication temperature increased to 620 °C (sample 620-2-FC), some particles were observed as pointed out by white arrows in Fig. 3(b). Most of the particles were distributed in the matrix, and a small number of them were near or at the interface between B_4C and the matrix. The EDS analysis indicated that the Mg content (12.82 at.%) of the particles was much higher than the mean Mg content (about 1.2 at.%) of the matrix, as shown in Fig. 3(c).

The EPMA results of Mg element distribution in samples 560-2-FC and 620-2-FC are shown in Fig. 4. It is clear that Mg element was uniformly distributed in the matrix when the fabrication temperature was 560 °C, but aggregated severely when the fabrication temperature was 620 °C.

Fig. 5 shows the XRD patterns of samples 560-2-FC and 620-2-FC. It can be seen that apart from Al and B_4C, the primary strengthening phase of 6061Al alloy, Mg_2Si, was detected clearly in sample 560-2-FC. However, the intensities of the Mg_2Si peaks were too weak to be detected in sample 620-2-FC. The main interfacial reaction product between Al and B_4C, Al_3BC, was revealed in sample 620-2-FC. Furthermore, two Mg containing phases ($MgAl_2O_4$ and MgB_7) and one Si containing phase (Al_4SiC_4), as the products of interfacial reactions involving alloying elements, were also detected in sample 620-2-FC. It is noted that the intensities of all the products involving alloying elements were much lower than those of Al_3BC in sample 620-2-FC, indicating the low contents of these phases.

3.2. Microstructural characterization of B_4C particles

As mentioned above, the peak intensities of the reaction products in the XRD patterns were very low and most XRD peaks were overlaid by others. It was hard to analyze the quantities of these phases in the composites fabricated at different parameters. Furthermore, there were still some tiny peaks that could not be confirmed only by the XRD patterns. For these reasons, B_4C particles were extracted from samples 560-2-FC, 560-10-FC and 620-2-FC.

Fig. 6 shows the higher magnification micrographs of samples 560-2-FC, 560-10-FC and 620-2-FC and the B_4C particles extracted from these samples. It was indicated that the microstructure of the composites showed different responses to the changes of the hot-pressing temperature or the holding time. For sample 560-2-FC with an HP temperature of 560 °C and a holding time of 2 h, the morphology of B_4C particles was still polygonal with blunt edge and low aspect ratio (Fig. 6(a) and (b)), just the same as the as-received B_4C (Fig. 1). For sample 560-10-FC with the same HP temperature and an extended holding time of 10 h, the morphology of the particles did not show a distinct change (Fig. 6(c) and (d)). However, for sample 620-2-FC with a higher HP temperature of 620 °C and a holding time of 2 h, as shown in Fig. 6(e) and (f), the morphology of B_4C particles was obviously different from the as-received B_4C or B_4C in samples 560-2-FC and 560-10-FC. The cusps of the particles were blunted severely and the sharp edges of the particles were serrated in sample 620-2-FC.

Moreover, some fine particles were observed on the surface of the B_4C particles extracted from all of these composites (Fig. 6(b), (d) and (f)). However, no changes were observed in the quantity and size of these particles for different hot-pressing parameters only by SEM images. The EDS analysis showed that the composition of these particles was close to $MgAl_2O_4$, which had already been proved to be the interfacial reaction product between Mg and the oxides in the B_4C/6061Al composites in our previous study [17].

Fig. 7 shows the XRD patterns of B_4C particles extracted from samples 560-2-FC, 560-10-FC and 620-2-FC. It can be seen that

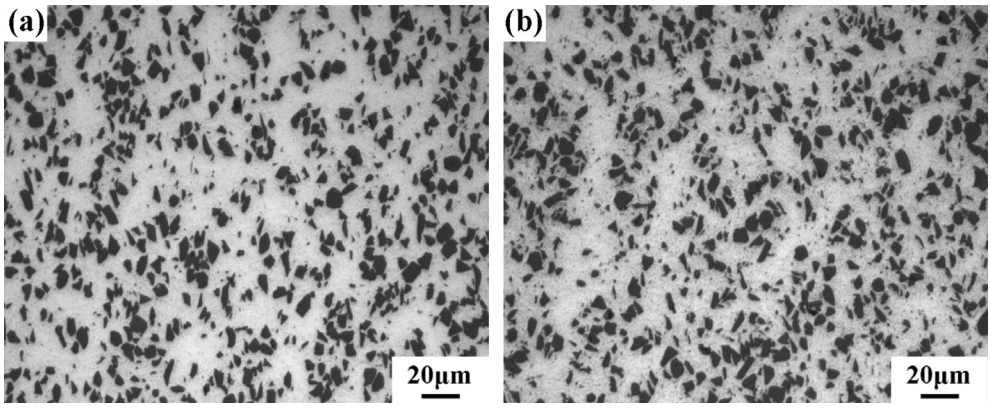

Fig. 2. OM micrographs of samples 560-2-FC and 620-2-FC.

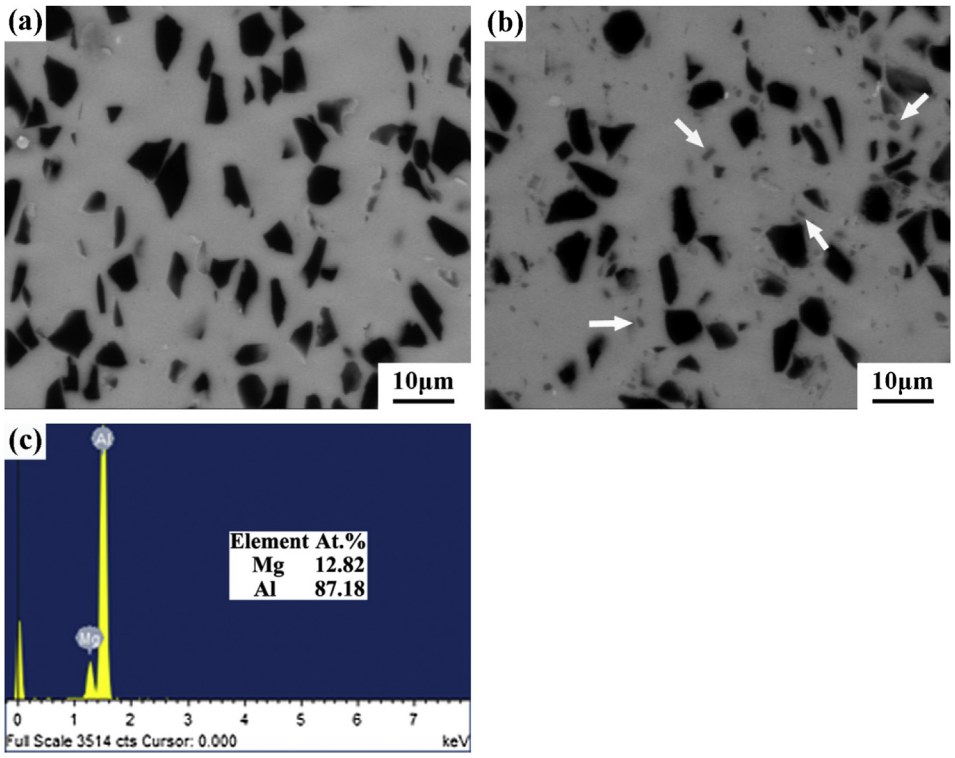

Fig. 3. SEM micrographs of samples (a) 560-2-FC and (b) 620-2-FC, and (c) EDS analysis of particles pointed out by white arrows in (b).

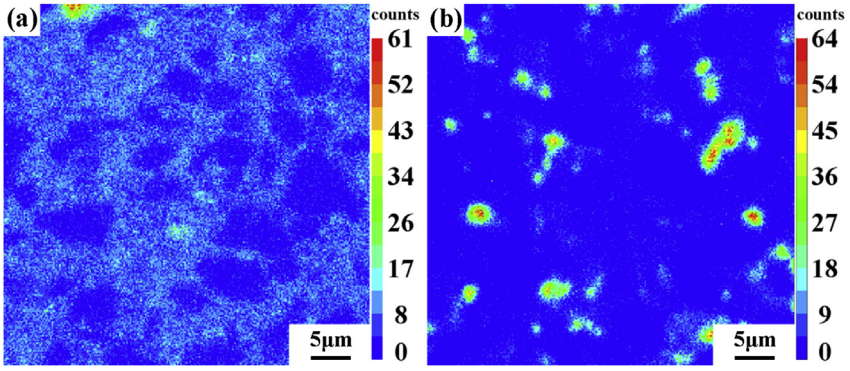

Fig. 4. Mg element distribution maps of samples 560-2-FC and 620-2-FC.

many peaks were observed apart from B_4C. These peaks were determined to be the Mg containing or Si containing phases. However, the type and the quantity of these phases were different for different hot-pressing parameters. When the hot-pressing temperature was 560 °C (samples 560-2-FC and 560-10-FC), $MgAl_2O_4$ was the only phase observed in the extracted B_4C particles. As the temperature increased to 620 °C, $MgAl_2O_4$ could still be detected. At the same time, $Mg_2B_2O_5$, $Mg_{0.78}Al_{0.75}B_{14}$, MgB_7 and Al_4SiC_4 were also observed in the extracted particles.

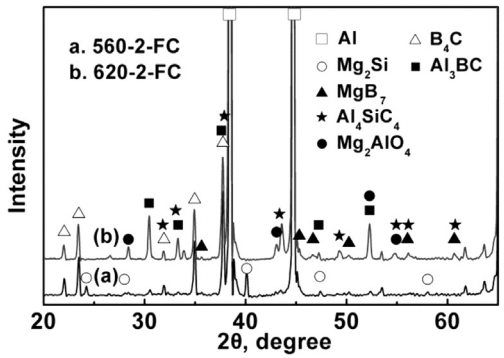

Fig. 5. XRD patterns of samples 560-2-FC (a) and 620-2-FC (b).

To evaluate the changing tendency of $MgAl_2O_4$ with the hot-pressing temperature and holding time, using the relative intensity of B_4C (021) and $MgAl_2O_4$ (400) planes, the relative intensity fractions of $MgAl_2O_4$ in the B_4C/6061Al composites can be calculated according to Refs. [18,19] and the results are listed in Table 3. It can be seen that the amount of $MgAl_2O_4$ increased with the prolongation of the holding time to 10 h (sample 560-2-FC to sample 560-10-FC). However, the amount of $MgAl_2O_4$ decreased as the hot-pressing temperature increased from 560 to 620 °C at a constant holding time of 2 h.

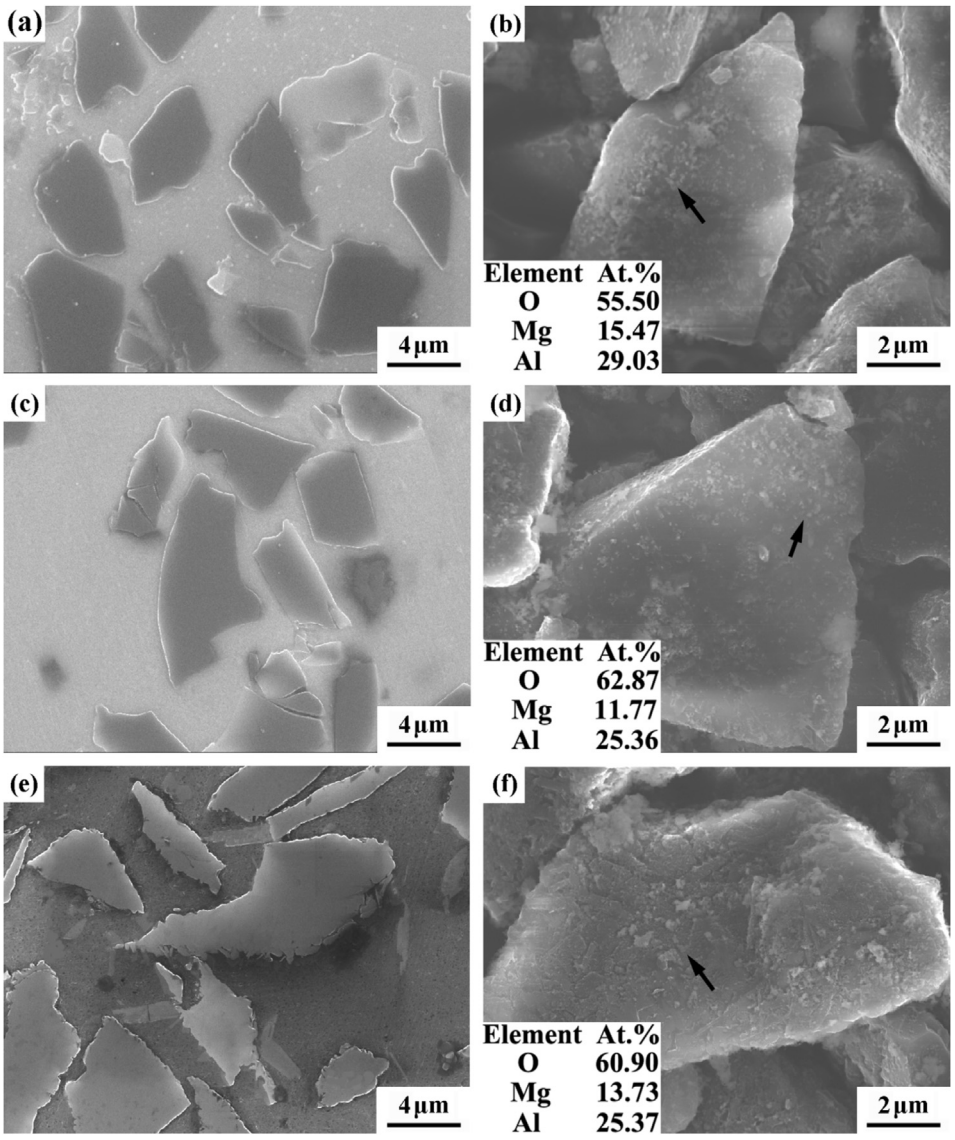

Fig. 6. SEM micrographs (a, c, e) and extracted particles (b, d, f) of samples 560-2-FC (a, b), 560-10-FC (c, d), and 620-2-FC (e, f).

3.3. *Interface characterization of B_4C/6061Al composites*

Fig. 8 shows the TEM images of samples 560-2-FC and 620-2-FC. It can be seen that the interface was very clean and the edge of the particle was intact and flat when the hot-pressing temperature was 560 °C (sample 560-2-FC, Fig. 8(a)), which is consistent with the SEM examinations of the extracted particles (Fig. 6(a) and (b)). At the same time, in accordance with the XRD result (Fig. 7), $MgAl_2O_4$ was the main reaction product in sample 560-2-FC and almost all $MgAl_2O_4$ was observed in the matrix of the composite rather than at the interface between B_4C particles and the matrix (Fig. 8(b)). The size of the $MgAl_2O_4$ particles was very small, just about 20–100 nm. The aggregation of $MgAl_2O_4$ particles was commonly observed.

However, the interface became very complicated at higher HP temperature of 620 °C (sample 620-2-FC, Fig. 8(c)). First, the sharp edges of B_4C particles were serrated. This is consistent with the SEM examinations (Fig. 6(e) and (f)). Second, the $MgAl_2O_4$ particles with a size of about 20–100 nm and the aggregated distribution were still observed in sample 620-2-FC (Fig. 8(d)). Different from those in sample 560-2-FC, these $MgAl_2O_4$ particles in sample 620-2-FC were located at both the matrix and the interfaces. Moreover, the aggregation of finer MgO particles with a size of less than 20 nm was observed near the B_4C particles, as indicated by a black circle in Fig. 8(e). Third, the reaction products between Al and B_4C, Al_3BC pointed out by black arrows in Fig. 8(f) and (g) and $Al_{12}BC_2$ pointed out by a black arrow in Fig. 8(h), were detected at the interface between B_4C particles and the matrix. The size of a single particle was approximately 200 nm.

With more detailed microstructural analysis, other interfacial reaction products involving Mg or Si elements were detected in sample 620-2-FC. Fig. 9 shows the location and type of these interfacial reaction products. First, MgB_7 with a size of 400 nm was detected at the B_4C/matrix interface (Fig. 9(a)). Second, $Mg_{0.78}Al_{0.75}B_{14}$ with a size of about 50 nm was observed in the matrix (Fig. 9(b)). Third, Al_4SiC_4 with a size of about 300 nm were found both at the B_4C/matrix interface and in the matrix as pointed out by black arrows in Fig. 9(c) and (d). Considering the limited amount of Mg element, the formation of MgB_7 and $Mg_{0.78}Al_{0.75}B_{14}$ may be attributed to the fact that the amount of $MgAl_2O_4$ present decreased as the hot-pressing temperature increased from 560 to

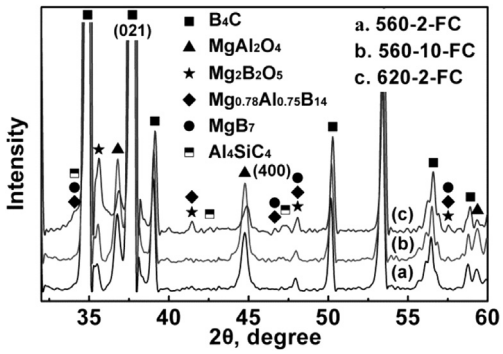

Fig. 7. XRD patterns of extracted particles from samples 560-2-FC (a), 560-10-FC (b), and 620-2-FC (c).

Table 3
The relative fractions of $MgAl_2O_4$ calculated based on B_4C (021) and $MgAl_2O_4$ (400) in the extracted particles from samples 560-2-FC, 560-10-FC and 620-2-FC.

560-2-FC	560-10-FC	620-2-FC
2.200%	2.952%	1.091%

620 °C at a constant holding time of 2 h.

3.4. Quenching of B_4C/6061Al composites

Fig. 10 shows the SIMS results of samples 620-0-WQ, 620-0.5-WQ, 620-1-WQ and 620-2-WQ. A little Mg segregation can be observed in sample 620-0-WQ, indicating that interfacial reactions have already occurred during increasing the temperature to 620 °C. With the increase of the holding time at 620 °C after HP, the segregation degree of Mg increased as shown in Fig. 10(a), (c), (e) and (g). Severe segregation of Mg formed when the holding time reached 1 h (Fig. 10(e)). With further increasing the holding time to 2 h (Fig. 10(g)), very tiny change of Mg segregation was observed. This indicates that the interfacial reactions involving Mg almost finished when the holding time reached 1 h at 620 °C. The segregation of Si showed different behavior with the increase of the holding time. No segregation of Si was detected with the holding time increased from 0 to 1 h as shown in Fig. 10(b), (d) and (f). However, the segregation of Si appeared when the holding time was prolonged from 1 to 2 h, resulting in significantly reduced amount of Si uniformly distributed in the matrix.

In summary, the segregation of both Mg and Si was detected when the holding time reached 2 h in the B_4C/6061Al composites fabricated at 620 °C. However, the responses of Mg and Si to the holding time were different. It implies that the segregation of these two elements was related to each other. With the prolongation of the holding time, the segregation of Mg first occurred. Si started to segregate only when the segregation of Mg almost finished, indicating that the segregation of Si was controlled by Mg. The segregation process of Mg and Si was related to the growth of the reaction products as stated above. It could be considered that the interfacial reactions involving Si were controlled by the reactions involving Mg. The reactions involving Si occurred only after Mg was almost completely consumed.

3.5. Age-hardening abilities of B_4C/6061Al composites

Fig. 11 shows the artificial aging curves and age-hardening abilities of samples 560-2-FC, 560-10-FC and 620-2-FC. The age-hardening ability was defined by a difference between peak aging hardness and solution hardness. It can be seen from Fig. 11(a) that all these three composites showed the typical aging curves similar to the 6061Al alloy and reached the peak aging hardness at an aging time of 6 h. However, significant differences were observed in the age-hardening abilities of these composites as shown in Fig. 11(b). With the HP parameter of 560 °C and 2 h, sample 560-2-FC showed the highest age-hardening ability, with a value of 38 HRB. When prolonging the holding time from 2 to 10 h (sample 560-10-FC), the age-hardening ability decreased by about 24% (from 38 to 29 HRB). However, the age-hardening almost completely disappeared with a hardness increase of only 3 HRB when the HP temperature increased to 620 °C with the holding time of 2 h (sample 620-2-FC). This indicates that the HP temperature, rather than the holding time, had the major influence on the age-hardening ability of the B_4C/6061Al composites.

4. Discussion

4.1. Thermal and dynamic analysis of interfacial reactions

In this study, XRD and TEM results showed that $MgAl_2O_4$ was the only reaction product in the B_4C/6061Al composites pressed at 560 °C. The type of the products did not change even when the holding time was prolonged from 2 to 10 h. However, many new reaction products were detected at 620 °C with a holding time of 2 h, such as Al_3BC, MgO, MgB_7, Al_4SiC_4 and so on. This indicates that the HP temperature not only controlled the extent of the reactions but also determined the reaction type. When the HP temperature was 620 °C, the main reactions occurred during HP as follows:

$$3Al + B_4C = Al_3BC + 3B \quad (1)$$

$$Al + 3B_4C = AlB_{12}C_2 + C \quad (2)$$

$$2Mg + O_2 = 2MgO \quad (3)$$

$$3Mg + B_2O_3 = 3MgO + 2B \quad (4)$$

$$3Mg + Al_2O_3 = 3MgO + 2Al \quad (5)$$

$$3Mg + 4Al_2O_3 = 3MgAl_2O_4 + 2Al \quad (6)$$

$$Mg + 7B = MgB_7 \quad (7)$$

$$Al + Si + 4C = Al_4SiC_4 \quad (8)$$

According to the thermodynamic data, the relationship between the standard Gibbs free-energy variation (ΔG_n^0) and temperature (T) of these reactions can be expressed by:

$$\Delta G_n^0 = A + BT \quad (9)$$

The value of A and B could be obtained from the thermodynamic data. By means of Eq. (9), the value of ΔG_n^0 of reactions (3)–(8) at different temperatures was calculated and the results are shown in Fig. 12. Because of the absence of the thermodynamic data, it was hard to calculate the value of ΔG_n^0 of reactions (1) and (2). It could be seen from Fig. 12 that all the value of ΔG_n^0 of reactions (3)–(8) was negative, indicating that these reactions had the thermodynamic driving force and could occur spontaneously at the hot temperatures used in this study.

However, different reaction products were generated at different temperatures as shown above, indicating that the reaction type varied with the HP temperature. According to the reaction

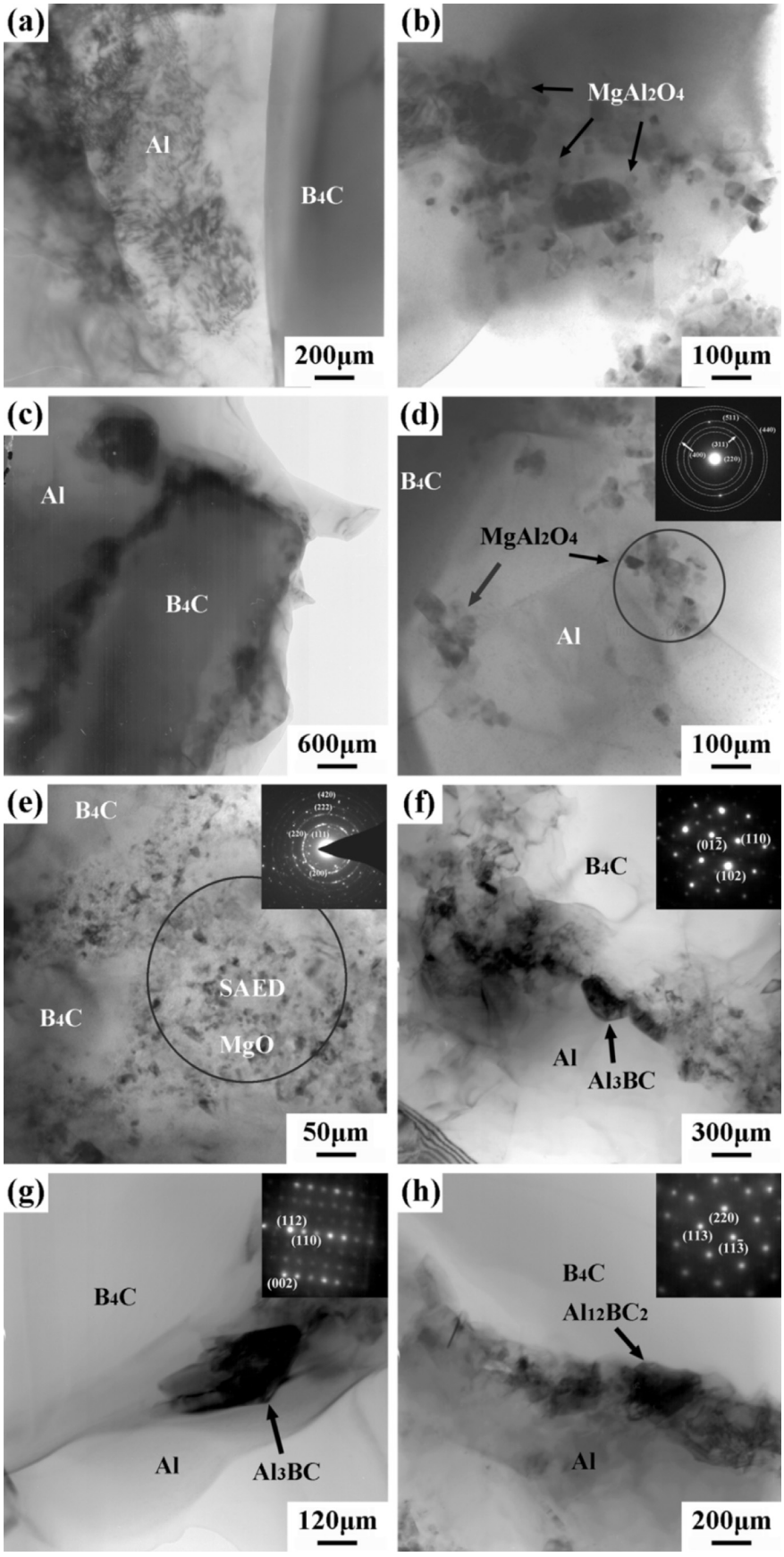

Fig. 8. TEM micrographs of samples 560-2-FC (a, b) and 620-2-FC (c, d, e, f, g, h). The insets show selected area electron diffraction patterns (SAED) of corresponding phases pointed out by black arrows.

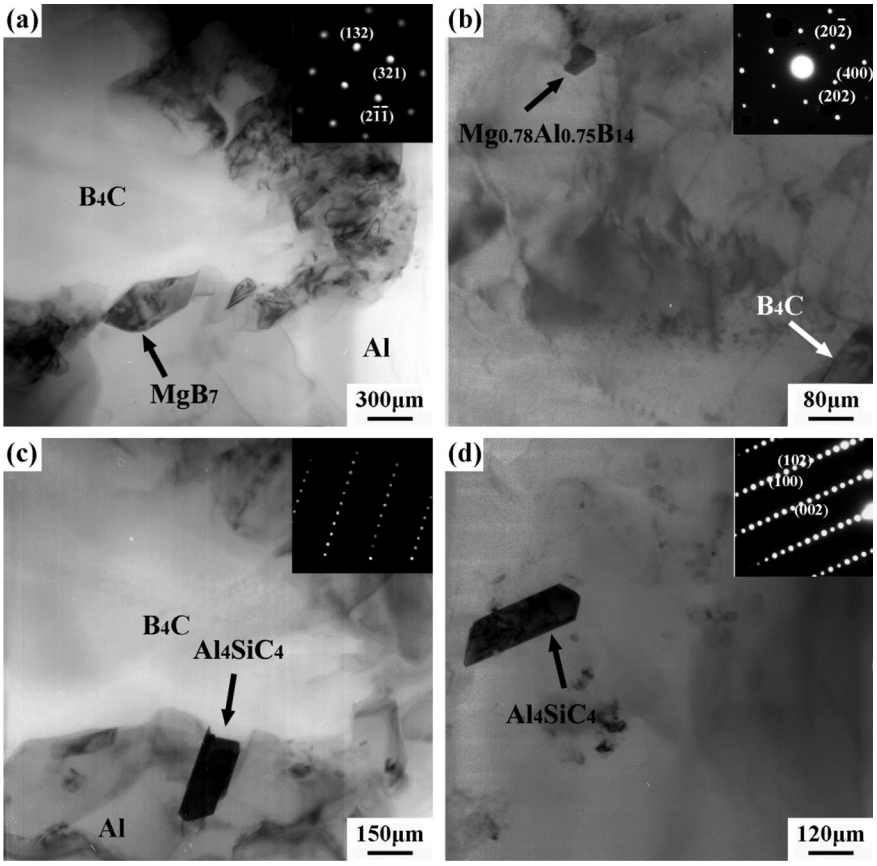

Fig. 9. Other interface products involving Mg and Si in sample 620-2-FC: (a) MgB_7, (b) $Mg_{0.78}Al_{0.75}B_{14}$, (c, d) Al_4SiC_4 with insets showing the corresponding SAED.

products and equations, the reactions involving Mg or Si (reactions (3)–(8)) could be divided into two groups. The first group, including reactions (3)–(6), could be defined as the oxidation of Mg which meant the reactions involving Mg and O elements. The main products were MgO and $MgAl_2O_4$. The source of "O" element could be the oxides in the B_4C powders, the Al_2O_3 film on the Al particles and the moisture adsorbed onto the powder particles. These reactions occurred both at 560 and 620 °C. The quantity of the products was larger at 560 °C.

The second group of reactions included reactions (7) and (8) which only occurred at 620 °C and where B or C was the element participating in the reactions. It should be pointed out that no free B or C was added into the composites. Therefore, other resources were required to supply B or C for maintaining these reactions. In this case, the supply of B or C was the critical issue to activate reactions (7) and (8). The activation of these reactions led to different interfacial reaction mechanisms of the B_4C/6061Al composites at different temperatures.

Reactions (1) and (2) are the reactions between Al and B_4C in the Al–B_4C system. The reaction between Al and B_4C has already been proven by some researchers [10,12–14]. It was mostly considered that the reaction between pure Al and B_4C could not occur until the temperature was up to 660 °C, which is the melting point of Al [10]. However, recent research found that the Al–B_4C reactions could occur below 600 °C. i.e., in solid state, after an extended holding time [12]. In this study, the Al–B_4C reactions obviously occurred at 620 °C with a holding time of only 2 h. This should be attributed to the existence of the liquid during the fabrication of the composite. It is well known that the formation of liquid phase was a critical issue for the fabrication and the interfacial reaction of AMCs by PM technique [20,21]. In a reaction system, the existence of the liquid phase would greatly facilitate the element diffusion, leading to a much faster reaction rate compared to a complete solid-state reaction.

As mentioned above, the addition of Mg and Si was 1 and 0.65 wt% in this study, respectively. According to the Al–Mg–Si phase diagram, the amount of the liquid phase could be calculated as about 1.2 and 16 wt% for 6061Al alloy at 560 and 620 °C, respectively. Correspondingly, the amount of liquid phase would be 0.96 wt% and 12.8 wt% for 20 wt%B_4C/6061Al composites. For the composite fabricated at 620 °C, 12.8 wt% liquid phase would approximately form a liquid net after the hot-pressing of the composites, facilitating the reaction between pure Al and B_4C.

Because of the negligible amount of liquid phase, the interfacial reaction could be regarded as the solid-state reaction at 560 °C. Schaffer and McCormick [22] suggested that the solid-state reaction rate was controlled by diffusion of the reactants through the product materials. The reaction of solids was therefore dependent on the initial contact area and the factors that influence the diffusion rate, such as defect density, local temperature and product morphology. In a thermally activated system, the reactant locations usually remain unchanged and are spatially separated by the reactive products during the course of the reaction, resulting in a lower diffusion rate and then a lower solid-state reaction rate. This may be the reason that reactions (1) and (2) were not observed at 560 °C, although these reactions were feasible in thermodynamics. Correspondingly, reactions (7) and (8) failed to be activated because of the lack of B and C elements generated by reactions (1) and (2).

When the HP temperature was 620 °C, the sufficient contact of B_4C and all the elements in 6061Al alloy was basically achieved by the multi-element liquid phase net and the reaction rate was

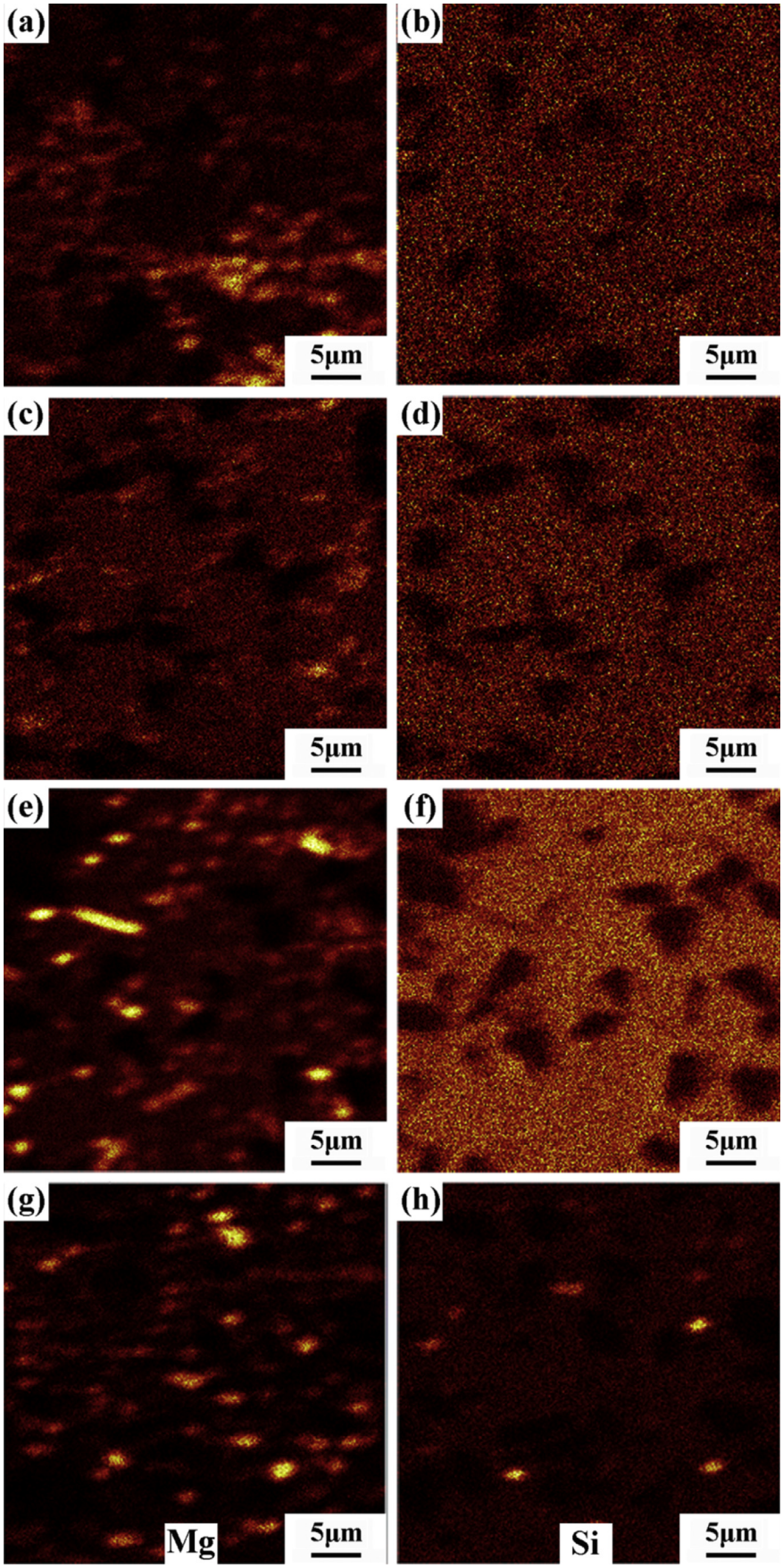

Fig. 10. The distribution of Mg (a, c, e, g) and Si (b, d, f, h) in samples 620-0-WQ (a, b), 620-0.5-WQ (c, d), 620-1-WQ (e, f) and 620-2-WQ (g, h).

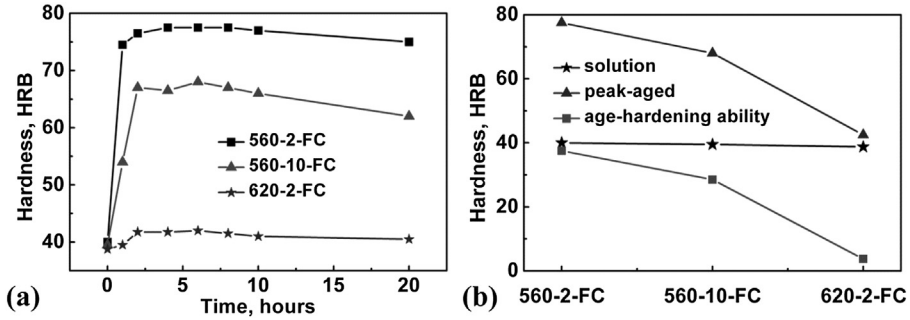

Fig. 11. (a) Artificial aging curves and (b) age-hardening abilities of samples 560-2-FC, 560-10-FC, and 620-2-FC.

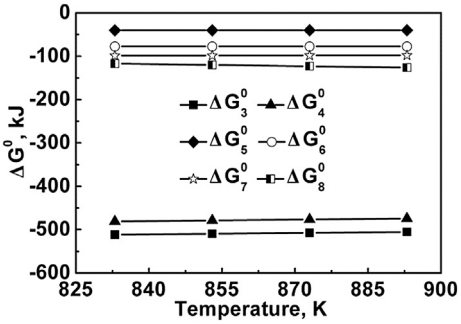

Fig. 12. Standard Gibbs free-energy variations of possible interfacial reactions in B_4C/6061Al composites.

accelerated by the increase of the temperature. These significantly facilitated the occurrence of all reactions, especially for reactions (1) and (2). Accordingly, a lot of free B and C were generated, leading to the activation of reactions (7) and (8).

4.2. Mechanism and sequence of interfacial reactions

As discussed above, the reaction mechanism would change with the temperature. All the reactions involving Mg and Si elements could be divided into two groups: the oxidation of Mg as reactions (3)–(6) and other reactions involving Mg and Si as reactions (7) and (8). Correspondingly, the reaction mechanism also could be divided into two series.

First, the oxidation of Mg occurred both at 560 °C and 620 °C and the final products were MgO and $MgAl_2O_4$. The formation of $MgAl_2O_4$ and MgO has also been reported by other investigators in the B_4C/Al composites and other composite systems, such as Al/SiC [6–8], Al/Al_2O_3 [4,9], Al/BN [23], etc.

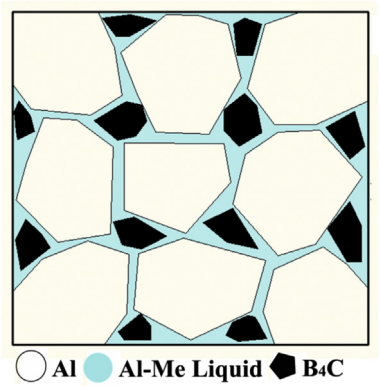

Fig. 13. Schematic diagrams after hot-pressing at 620 °C for 20 wt%B_4C/6061Al composite.

Second, reactions (7) and (8) only occurred at 620 °C and the activation of these reactions was controlled by reactions (1) and (2). Fig. 13 shows the schematic diagram after the hot-pressing of the composites with the multi-element liquid phase net at 620 °C. It can be seen that all the B_4C and Al particles were surrounded by the liquid phase. As mentioned above, this liquid phase was composed of Al, Mg and Si elements. With the prolongation of the holding time, reaction (1) would occur. Thus, free B was generated and then diffused into the liquid phase. In this case, B, Al, Mg and Si were the main elements in the liquid phase. So the chemical reactions among these elements would occur in this liquid system.

Based on the principle of the electronegativity, the reaction would occur between two elements with the larger electronegativity difference in a chemical system. In this study, the element in the liquid could be sorted according to the electronegativity: B > Si > Al > Mg. Thus, B and Mg were the two elements to compound most easily. The reactions between B and Mg occurred to form MgB_x (MgB_7 in Figs. 5, 7 and 9). The reactions involving Mg, B and Al also occurred to form $Mg_xAl_yB_z$ ($Mg_{0.78}Al_{0.75}B_{14}$ in Figs. 7 and 9).

With the prolongation of the holding time at 620 °C, almost all the Mg element was consumed. However, reaction (1) still went ahead leading to the redundancy of B in the liquid phase. Because of the very low solubility of B in Al liquid [9], reaction (1) would be suppressed and reaction (2) occurred, leading to the generation of free C into the liquid phase. In this case, C, B, Al and Si were the main elements in the liquid phase and could be sorted with the electronegativity: C > B > Si > Al. Thus, C and Al were the two elements to compound most easily. The reaction between C and Al should produce Al_4C_3. However, Al_4C_3 was not detected in this study. A ternary phase, Al_4SiC_4, was instead observed as shown in Figs. 5, 7 and 9.

It has been reported that the generation of Al_4C_3 could be suppressed in the Al–Si–SiC system when the content of Si was more than 8.5% at 620 °C [24]. For the present 6061 (Al–1Mg–0.65Si, wt %) alloy, the Si contents in the liquid phase at the starting stage and the equilibrium state at 620 °C were about 30 wt% and 5 wt%, respectively, according to the phase diagram. Thus the Si content in the liquid phase could be more than 8.5% for a relatively long time in this study, although the nominal composition of Si was only 0.65 wt%. It may be the reason that no Al_4C_3 was observed and Al_4SiC_4 was generated according to reaction (8). The generation of Al_4SiC_4 at lower temperatures has been reported in Al–Ti_3SiC_2 system [25].

The sequence of the reactions involving Mg and Si was also supported by the element distribution results shown in Fig. 10. The segregation of Si occurred only when the segregation of Mg

finished. This indicates that the reaction involving Si was controlled by the reactions involving Mg.

AlB_2 is another common product in the Al–B_4C system, which has already been reported by many investigators [10,13]. However, it was not detected in this study. That may be attributed to the insufficient of the holding time.

4.3. Age-hardening abilities

It is well known that Mg_2Si is essential for age-hardening of 6061Al alloy. However, distinct interfacial reactions occurring in the B_4C/6061Al composites led to consumption of Mg and Si. This would decrease quantity of Mg_2Si precipitates during the aging treatment, thereby deteriorating the age-hardening ability of the composites. Because the reaction involving Si occurred only after the reactions involving Mg finished, the consumption of Mg should be the main factor for the deterioration of the age-hardening ability of the B_4C/6061Al composites.

The amount of Mg element in the 6061Al alloy is only 1 wt% and the amount of the oxides in the raw B_4C and Al powders are also limited as shown in Table 1. As mentioned above, the oxidation of Mg was the first reaction occurring in the B_4C/6061Al composites. Thus, part of the consumption of Mg element would be related to the oxidation of Mg. According to the rough calculation, more than half amount of free Mg would be left when the oxidation of Mg was over.

When the hot-pressing parameters were 560 °C and 2 h, the B_4C/6061Al composite exhibited high age-hardening ability as shown in Fig. 11. It may be attributed to that only a small amount of Mg element was consumed in the reactions between Mg and the oxides. A large amount of remaining Mg element precipitated as Mg_2Si during the aging treatment to improve the hardness of the composite. With prolonging the holding time to 10 h at 560 °C, which led to significant increase of the oxidation of Mg, the age-hardening ability showed a slight decrease. However, with the elevation of the hot-pressing temperature from 560 to 620 °C, which led to the activation of the reactions involving B and Mg, the age-hardening ability showed a significant decrease. Therefore, it should be concluded that the reactions involving B and Mg rather than the oxidation of Mg were the main reasons for the deterioration of the age-hardening ability of B_4C/6061Al composites at 620 °C.

5. Conclusions

1. Complicated interfacial reactions occurred in the B_4C/6061Al composites and the main products were Al_3BC, $MgAl_2O_4$, MgO, MgB_7, $Mg_{0.78}Al_{0.75}B_{14}$, $AlB_{12}C_2$ and Al_4SiC_4. The formation of $MgAl_2O_4$, MgB_7 and $Mg_{0.78}Al_{0.75}B_{14}$ led to severe depletion of the free Mg element and evidently deteriorated the aging-hardenability of the B_4C/6061Al composites.
2. The reactions involving Mg and Si could be divided into two series. The oxidation of Mg occurred at 560 and 620 °C with the main products being $MgAl_2O_4$ and MgO. Other reactions only occurred at 620 °C with the main products being MgB_7, $Mg_{0.78}Al_{0.75}B_{14}$, $AlB_{12}C_2$ and Al_4SiC_4.
3. The existence of the liquid phase at 620 °C resulted in the occurrence of reactions between Al and B_4C and free B generated got into the liquid phase. Then the reactions involving B and Mg occurred. Only if the reactions containing B and Mg were completed, the reaction between Al, Si and C occurred.
4. The reactions involving B and Mg rather than the oxidation of Mg or the reaction involving Si were the main reasons for the consumption of Mg and the deterioration of age-hardening ability of the B_4C/6061Al composites at 620 °C.

Acknowledgments

The authors gratefully acknowledge the support of the National Basic Research Program of China under grant No. 2012CB619600.

References

[1] W.M. Zhong, G. Lesperance, M. Suery, Mater. Sci. Eng. A 26 (1995) 2637–2649.
[2] L. Salvo, G. Lesperance, M. Suery, J.G. Legoux, Mater. Sci. Eng. A 177 (1994) 173–183.
[3] J.C. Lee, J.P. Ahn, Z.L. Shi, J.H. Shim, H.I. Lee, Metal. Mater. Trans. A 32 (2001) 1541–1550.
[4] K.B. Lee, Y.S. Kim, H. Kwon, Metal. Mater. Trans. A 29 (1998) 3087–3095.
[5] G.G. Sozhamannan, S.B. Prabu, Mater. Charact. 60 (2009) 986–990.
[6] A. Urena, E.E. Martinez, P. Rodrigo, L. Gil, Compos. Sci. Technol. 64 (2004) 1843–1854.
[7] J.H. Jeong, Y. Kim, J.C. Lee, Metal. Mater. Trans. A 34A (2003) 1361–1369.
[8] J. Lee, H. Lee, J. Ahn, Z. Shi, Y. Kim, Metal. Mater. Trans. A 31A (2000) 2361–2368.
[9] H.S. Chu, K.S. Liu, J.W. Yeh, Scr. Mater. 45 (2001) 541–546.
[10] J.C. Viala, J. Bouix, G. Gonzalez, C. Esnouf, J. Mater. Sci. 32 (1997) 4559–4573.
[11] A.J. Pyzik, D.R. Beaman, J. Am. Ceram. Soc. 78 (1995) 305–312.
[12] M. Kubota, J. Alloys Compd. 504 (Suppl. 1) (2010) S319–S322.
[13] A.R. Kennedy, J. Mater. Sci. 37 (2002) 317–323.
[14] K.B. Lee, H.S. Sim, S.Y. Cho, H. Kwon, Mater. Sci. Eng. A 302 (2001) 227–234.
[15] C. Nie, J. Gu, J. Liu, D. Zhang, J. Alloys Compd. 454 (2008) 118–122.
[16] H.M. Hu, E.J. Lavernia, W.C. Harrigan, J. Kajuch, S.R. Nutt, Mater. Sci. Eng. A 297 (2001) 94–104.
[17] Y.Z. Li, Q.Z. Wang, W.G. Wang, B.L. Xiao, Z.Y. Ma, Mater. Sci. Eng. A 620 (2015) 445–453.
[18] Q.C. Jiang, H.Y. Wang, B.X. Ma, Y. Wang, F. Zhao, J. Alloys Compd. 386 (2005) 177–181.
[19] N.L. Yue, L. Lu, M.O. Lai, Compos. Struct. 47 (1999) 691–694.
[20] Q. Zhang, B.L. Xiao, Z.Y. Liu, Z.Y. Ma, J. Mater. Sci. 46 (2011) 6783–6793.
[21] B. Ogel, R. Gurbuz, Mater. Sci. Eng. A 301 (2001) 213–220.
[22] G.B. Schaffer, P.G. McCormick, Metal. Mater. Trans. A 23 (1992) 1285–1290.
[23] K.B. Lee, J.P. Ahn, H. Kwon, Metal. Mater. Trans. A 32A (2001) 1007–2018.
[24] D.J. Lloyd, Compos. Sci. Technol. 35 (1989) 159–179.
[25] W.L. Gu, C.K. Yan, Y.C. Zhou, Scr. Mater. 49 (2003) 1075–1080.